

Experimental study of the influence of anisotropy on the inertial scales of turbulence

**KELKEN CHANG, GREGORY P. BEWLEY[†]
AND EBERHARD BODENSCHATZ**

Max Planck Institute for Dynamics and Self-Organization, 37077 Göttingen, Germany

International Collaboration for Turbulence Research

(Received 26 January 2011 and in revised form 25 October 2018)

We ask whether the scaling exponents or the Kolmogorov constants depend on the anisotropy of the velocity fluctuations in a turbulent flow with no shear. According to our experiment, the answer is no for the Eulerian second-order transverse velocity structure function. The experiment consisted of 32 loudspeaker-driven jets pointed toward the centre of a spherical chamber. We generated anisotropy by controlling the strengths of the jets. We found that the form of the anisotropy of the velocity fluctuations was the same as that in the strength of the jets. We then varied the anisotropy, as measured by the ratio of axial to radial root-mean-square (RMS) velocity fluctuations, between 0.6 and 2.3. The Reynolds number was approximately constant at around $R_\lambda = 481$. In a central volume with a radius of 50 mm, the turbulence was approximately homogeneous, axisymmetric, and had no shear and no mean flow. We observed that the scaling exponent of the structure function was 0.70 ± 0.03 , independent of the anisotropy and regardless of the direction in which we measured it. The Kolmogorov constant, C_2 , was also independent of direction and anisotropy to within the experimental error of 4%.

[†] Email address for correspondence: gregory.bewley@ds.mpg.de

1. Introduction

Theories of turbulence that give precise predictions apply by mathematical necessity to statistically isotropic flows. A conjecture, due to Kolmogorov (1941), is that flows characterised by large enough Reynolds numbers are locally isotropic, or isotropic at small scales, even in the presence of anisotropy at larger scales. Understanding the way turbulence tends to local isotropy from various states of anisotropy remains an important challenge in the study of turbulence. Its importance lies in the fact that almost all flows in the natural world and in technical applications are anisotropic, and not of sufficiently high Reynolds numbers for its influence to be neglected. Any useful theory or model of turbulence should therefore incorporate anisotropy, and the purpose of this investigation is to provide test cases for such theories.

The conjecture of local isotropy has received much attention (e.g. Saddoughi & Veeravalli 1994; Kurien & Sreenivasan 2001; Biferale & Procaccia 2005), and has been tested in flows with various kinds of anisotropy. Anisotropy can arise in different ways, for example through spatial variation of the mean flow (e.g. Tavoularis & Corrsin 1981), or through anisotropy in the velocity fluctuations. These different forms of anisotropy might have different effects on the small scales of turbulence. No test has been performed previously to isolate the influence of anisotropy in the fluctuations only, without also introducing shear. Our task was to create a device with which we could do this. We show that it is possible in a single apparatus to produce turbulence with negligible shear, and with a chosen level of anisotropy on the large scale. With the apparatus, we tested the validity of the hypothesis of local isotropy under increasingly anisotropic conditions.

We produced anisotropy in the velocity fluctuations by introducing an asymmetry in the agitation of the turbulence. Evidence suggests that there is a causal relationship between asymmetry in the agitation of turbulence, and anisotropy in the energy-containing

scales of turbulence. For example, asymmetry and anisotropy are present at the same time in turbulent jets (e.g. Hussein, Capp & George 1994), Taylor-Couette flows (e.g. Andereck, Liu & Swinney 1986), and wind tunnels with specially designed shear generators (e.g. Tavoularis & Corrsin 1981). Turbulence produced by computer simulation can also be forced in an asymmetric way; Yeung & Brasseur (1991) studied the influence of this asymmetry. One exception is the turbulence produced by a grid in a wind tunnel with a contraction, where the axis of the tunnel introduces an asymmetry, yet the turbulence produced can be nearly isotropic, but decaying (Comte-Bellot & Corrsin 1966). There is also a pattern in the relationship between asymmetry of the forcing and anisotropy of the turbulence. Machines with a single axis of symmetry, such as the von Kármán flow (e.g. Ouellette *et al.* 2006) and wind tunnels (e.g. Staicu, Vorselaars & van de Water 2003), produced axisymmetric turbulence. Machines with more axes, such as the one developed by Hwang & Eaton (2004), produced isotropic turbulence. A careful study by Zimmermann *et al.* (2010) showed that six axes were sufficient to produce turbulence without a preferred direction. Our machine had 16 axes.

We generated both isotropic and axisymmetric flows. The apparatus worked by modulating the relative intensity of 32 mixers distributed over a sphere. When all the mixers were driven with the same intensity, isotropic turbulence resulted. We introduced a preferred axis by driving mixers near one of the 16 axes of the machine either more strongly or more weakly than the other mixers. This produced anisotropy in the turbulence. The geometric form of the apparatus was inspired by the one of Zimmermann *et al.* (2010), except that ours used 32 mixers instead of their 12, and air as the working fluid instead of water. Our mixers were loudspeakers coupled to nozzles; the diaphragm of the loudspeaker pushed and pulled air through an orifice, which formed a turbulent jet. This technique for mixing air was invented by Hwang & Eaton (2004), though our imple-

mentation differs in several details, described below. We used laser Doppler velocimetry (LDV) to measure the fluid velocity near the centre of the apparatus.

We measured the influence of anisotropy on velocity structure functions, which are the moments of velocity differences across two points separated in space. The second order structure function is

$$D_{ij}(\mathbf{r}) = \langle (u_i(\mathbf{r}) - u_i(0))(u_j(\mathbf{r}) - u_j(0)) \rangle, \quad (1.1)$$

where $u_i(\mathbf{r})$ is the fluctuation of the i -th component of the velocity at location \mathbf{r} and $\langle \cdot \rangle$ denotes temporal averaging. Local isotropy demands that for small enough \mathbf{r} and large enough Reynolds number, the structure function is isotropic. In this case it can be written in terms of a single independent scalar function.

Kolmogorov (1941) surmised that in the inertial subrange, where he thought that neither the viscosity nor the large-scales would influence the dynamics, the structure functions follow a power law as a function of spatial separation. For representative parts of the structure function tensor given in equation 1.1, this can be written

$$D_{zz}(r_1) \equiv \langle (u_z(r_1) - u_z(0))^2 \rangle = \frac{4}{3} C_2^{(r)} (\epsilon r_1)^{\zeta_2^{(r)}}, \quad (1.2)$$

$$D_{r_2 r_2}(z) \equiv \langle (u_{r_2}(z) - u_{r_2}(0))^2 \rangle = \frac{4}{3} C_2^{(z)} (\epsilon z)^{\zeta_2^{(z)}}. \quad (1.3)$$

These functions are called transverse because the velocities, u_z and u_{r_2} , are perpendicular to the vectors pointing from 0 to r_1 and from 0 to z , respectively. We have introduced a certain coordinate system that we describe later. Here, ϵ is the energy dissipation rate per unit mass, the dimensionless constants, $C_2^{(r)}$ and $C_2^{(z)}$, are called Kolmogorov constants, and the scaling exponents, $\zeta_2^{(r)}$ and $\zeta_2^{(z)}$, both equal $2/3^{rds}$ according to Kolmogorov (1941) for locally isotropic turbulence. The Kolmogorov constants are also equal to each other if the turbulence is locally isotropic, but their value must be determined by experiment. It is interesting to note that the corresponding Kolmogorov constants for the

Lagrangian structure function vary with angle by more than 20% at a Reynolds numbers of 815 in an anisotropic von Kármán swirling flow (Ouellette *et al.* 2006). Our work addresses the angular dependence of the Eulerian C_2 , and is in part an extension of the above work.

One of our measures of anisotropy is the ratio of Kolmogorov constants measured in the two different directions, $C_2^{(r)}/C_2^{(z)}$. Variation of this quantity could account for differences between published values of the Kolmogorov constant. Such differences are evident in Sreenivasan (1995), for example, where values for the constant were collected from various experiments and found differ from each other with a standard deviation of about 10%. Could it be that different experiments measured different values for the Kolmogorov constant because they had different levels of anisotropy, or else because they measured the constant in different directions? In our study, we found no dependence of the Kolmogorov constants on the anisotropy, as shown in section 4.

We also report on the difference between the scaling exponents measured in the two directions, $\Delta\zeta_2 = \zeta_2^{(z)} - \zeta_2^{(r)}$. Here, we sought to interpret the observation made by Shen & Warhaft (2002) that in anisotropic wind tunnel flows the scaling exponent in the cross-tunnel direction was about 0.1 smaller than the exponent in the direction of the mean flow. In our shearless, axisymmetric flow we found, in contrast, that the difference between the scaling exponents, $\Delta\zeta_2$, was zero to within the measurement accuracy. As is explained in section 4, we measured the exponents using the Extended Self-Similarity (ESS) technique introduced by Benzi *et al.* (1993).

In the following section 2, we describe the apparatus and techniques. In section 3, we show that we could control systematically the anisotropy of the turbulence, and report on the extent to which the turbulence had no shear and was axisymmetric. A reader

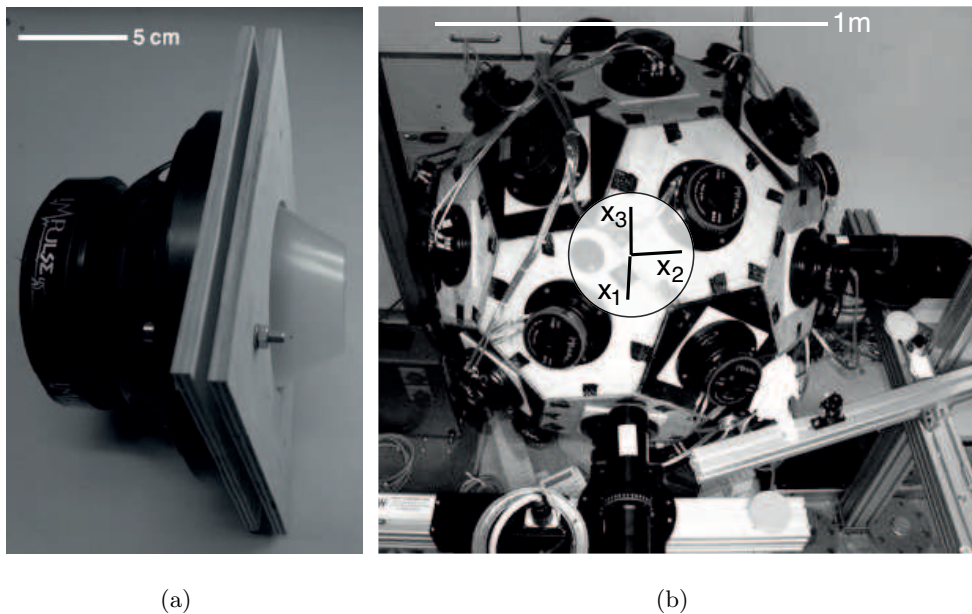


FIGURE 1. (a) The jet generator. (b) The layout of the turbulence chamber and the LDV probes (black cylinders), one near the bottom of the image, and one to the right. The one aligned with the x_1 -axis measures the components of particle velocities in both the x_2 and x_3 directions. The probe aligned with the x_2 axis measures velocities in either the x_1 or the x_3 direction.

with no interest in experimental detail can proceed to section 4, where we report on the measurements of structure functions. We conclude in section 5.

2. The Experiment

As shown in figure 1 (b), the turbulence chamber had the shape of a truncated icosahedron and a diameter of 99 cm. It was made of wood

joined together with nylon straps and glue. In the centre of each face a circular hole was cut for the jet generator. In addition, further holes adjacent to the jet generators were cut for optical access. As the shape is that of a soccer ball we will use this term from now on to describe the turbulence chamber.

As depicted in figure 1(a), the mixers were jets, similar in principle to those developed

for flow control applications (e.g. Glezer & Amitay 2002). A 150 W loudspeaker with a diameter of 16.5 cm and a uniform frequency response between 50 and 3000 Hz was mounted on each face of the soccer ball and pointed towards its centre. The loudspeakers were coupled to conical nozzles with opening angle 30° , length 4.3 cm, and orifice diameter 5 cm. When backing away from the orifice the diaphragm drew in air from all directions, while it blew it out in a single direction when moving toward the orifice. By driving the speaker sinusoidally, we generated a pulsating turbulent jet. The sound level inside the soccer ball was typically 135 dB, which corresponded to 0.2% of the measured turbulent kinetic energy. Thus we expect the sound to have a negligible effect on the turbulence and the measurements of velocity.

The flow chamber was similar to the ones described by Hwang & Eaton (2004), Webster, Brathwaite & Yen (2004) and Lu *et al.* (2008), who employed cubic Plexiglas boxes from which the corners were cut off. A speaker-driven jet was mounted at each of the eight cut-off corners, and pointed toward the centre of the chamber. The flow chamber of Warnaars, Hondzo & Carper (2006) was a rectangular Plexiglas box with two speakers placed at each square end of the box. A grid was placed in front of each speaker to excite small-scale turbulence. We compare the flow parameters in these apparatuses, as well as the one of Goepfert *et al.* (2010), in table 1.

We chose the signals that drove the loudspeakers to generate the desired anisotropy and low mean velocity in the flow. Figure 2 shows the power spectrum of the signal. The 50 Hz amplitude-modulated sine signals were digitally generated at a sampling frequency of 3 kHz. All speakers were driven in phase, and 50 Hz produced the strongest jets. The 50 Hz oscillation was not, however, detectable in the spectrum of the fluid velocities measured near the middle of the soccer ball. We modulated the amplitude of each driving signal with noise (Fox *et al.* 1988), though other forms of noise would probably also work.

	Hwang & Eaton (2004)	Webster <i>et al.</i> (2004)	Warnaars <i>et al.</i> (2006)	Lu <i>et al.</i> (2008)	Goepfert <i>et al.</i> (2010)	Present work
Geometry	Truncated cube	Truncated cube	Rectangular	Truncated cube	Octahedron	Truncated icosahedron
Flow medium	Air	Saltwater	Water	Air	Air	Air
σ (ms ⁻¹)	0.87	0.0097	0.00069	0.60	0.88	1.1
σ_u/σ_v	1.03	1.00	0.98	–	0.95	0.94
U/σ	0.022	0.07	–	–	0.03	0.04
ϵ (m ² s ⁻³)	11	2.5×10^{-5}	1.25×10^{-6}	1.4	5.8	6.7
η (μ m)	130	450	950	220	155	155
τ_η (ms)	1.2	200	1000	3.3	1.6	1.5
R_λ	220	68	5.9	260	250	481

TABLE 1. Chamber geometry and flow statistics from various speaker-driven flows. Symbols from top to bottom: RMS velocity fluctuations (σ), ratio of RMS velocity fluctuations (σ_u/σ_v), ratio of mean flow to RMS fluctuations (U/σ), energy dissipation rate (ϵ), Kolmogorov length scale (η), Kolmogorov time scale (τ_η), Taylor Reynolds number (R_λ). For each study, we give the highest Reynolds number, lowest mean flow and best isotropy reported by the authors. For our apparatus, we report only on data acquired under isotropic forcing.

The correlation time was 0.1 seconds, which was approximately equal to the large-scale eddy turn-over time, L/σ , L being a characteristic length scale describing the large-scale motions of the flow, and σ being the root mean squared (RMS) velocity fluctuations. This condition ensured that fluctuations in the energy input rate to the turbulence occurred on time scales equal to or faster than the turbulence decay time, so that the turbulence was in a steady state. In any case, we found that the statistical properties of the turbulence were insensitive to the correlation time.

To avoid mean flows, the amplitudes of each driving signal were adjusted so that the

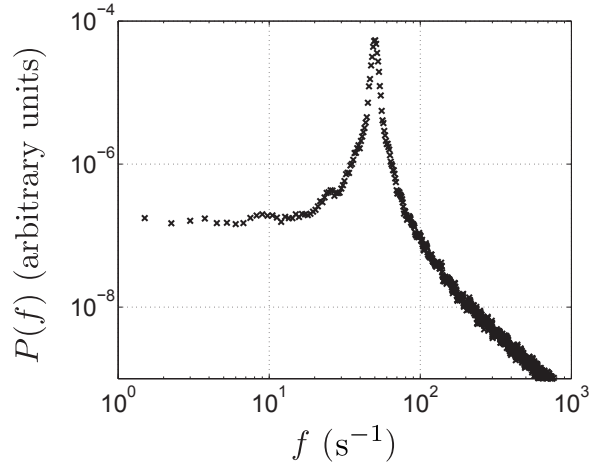


FIGURE 2. The power spectrum of the voltage applied to the loudspeakers.

sum of the amplitudes of all signals was zero. This also reduced the amplitude of the sound generated and the air exchange between the inside of the ball and the room.

We selected the desired anisotropy by separately adjusting the RMS amplitude of each speaker. As we restricted ourselves to cylindrically symmetric driving, the asymmetry could be characterised by the ratio of the axial amplitude, a_{axial} , to the radial amplitude, a_{radial} :

$$A = \frac{a_{\text{axial}}}{a_{\text{radial}}} . \quad (2.1)$$

A forcing is then described as exhibiting oblate spheroidal asymmetry when $0 < A < 1$, spherical symmetry when $A = 1$ and prolate spheroidal asymmetry when $A > 1$.

As we have 32 speakers distributed with icosahedral symmetry, the RMS amplitude for a given loudspeaker was set according to the following scheme. We defined an ellipsoid that had the same centre as the soccer ball, and whose major axis to minor axis ratio was A . We then calculated the intersection between the surface of the ellipsoid and the vector that pointed from the centre of the soccer ball to the centre of the given loudspeaker. The distance between this intersection and the centre of the soccer ball set the relative RMS amplitude for the given loudspeaker.

We characterised the flow using a TSI laser Doppler velocimetry (LDV) system. We used oil droplets as tracer particles, generated by a Palas AGF 10.0 aerosol generator. The droplets had a most probable diameter of about $3\ \mu\text{m}$, and a volume fraction of less than 10^{-7} . Droplets of this diameter settle in still air at $200\ \mu\text{m s}^{-1}$, which was much smaller than their RMS velocities in the turbulent flow. These oil droplets were passive tracers, since the Stokes number in our flow was very small (approximately 0.02) (e.g. Bewley, Sreenivasan & Lathrop 2008) and the accelerations of the turbulent flow were much larger than the acceleration of gravity (e.g. Voth *et al.* 2002).

As shown in figure 1(b), we used two LDV probes. One probe measured two components, and the other only one component of the velocity of individual tracer particles. The measurement volume was approximately ellipsoidal in shape, and was approximately $100\ \mu\text{m}$ in diameter and 2 mm in length, which allowed us to resolve scales larger than the dissipation scale of the turbulence. The mean data sampling rate was between 300 and 3000 samples per second, depending on the probe. We typically collected 2×10^6 data points per aspect ratio of the forcing and per spatial position of the probes.

LDV data are known to suffer from biases, since the system observes particles with larger velocities more often than those with smaller velocities (see e.g. Albrecht *et al.* 2003). We used the residence time weighting suggested by Buchhave (1975) and Buchhave, George Jr. & Lumley (1979) to correct our single point statistics. We did not correct for possible bias in our two-point statistics. To calculate the two-point statistics the velocity signals were first processed using a slotting technique, i.e., we searched for samples coming from each of the two probes with time separations falling within a temporal bin of 1 ms duration, and within each temporal bin, the data from each probe was averaged. Approximately $10^4 - 10^5$ points contributed to the statistics for each spatial separation.

We found that as long as the temporal bin was smaller than 15 ms the difference in the results was less than 1%.

Before we proceed to the measurements, we describe the coordinate system, which was fixed to the axis of symmetry of the turbulence. Please note that the coordinate system was not fixed in the laboratory frame, as is shown in figures 1 and 4. Axisymmetric turbulence has two principal axes. However, our measurement apparatus measured velocities only at points that lay along a single line in the laboratory frame. In order to sample the statistics of turbulence along both axes, we rotated the axis of symmetry of the turbulence by taking advantage of the symmetries of the soccer ball.

The soccer ball was oriented such that one of the symmetry axes of the forcing lay along $\theta = 107^\circ$ and $\phi = -4^\circ$, which is labelled as x'_1 in figure 4, and is close to the x_1 -axis. The other symmetry axis lay along $\theta = 4^\circ$ and $\phi = 180^\circ$, which is labelled as x'_3 in figure 4, and is close to the x_3 -axis. Because the primed and unprimed coordinate systems are close to each other, we do not distinguish between them in the rest of this paper. This simplification does not impact our conclusions, since we find no difference in the small-scale statistics between the two directions, despite the fact that they are approximately orthogonal.

Figure 3 shows the coordinate system, (r_1, r_2, z) , which was aligned with the symmetry axis of the forcing. The coordinate system has two orientations with respect to the laboratory coordinate system, corresponding to the two cases described above. Hereafter, ‘axial’ refers to both the direction of the velocity component measured along the axis of symmetry, and, in discussing two-point statistics, separations along the axis of symmetry. Similarly, ‘radial’ refers to both the direction of the velocity components perpendicular to the axis of symmetry, and to separations perpendicular to the axis of symmetry. In addition, we refer to two-point quantities whose separation vector lies along the axis of

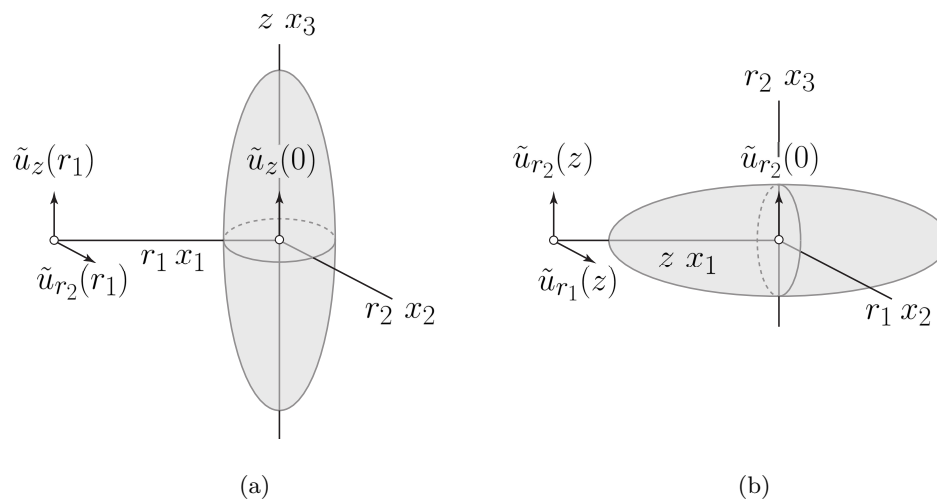


FIGURE 3. Orientations of the body coordinate system of the forcing with respect to the laboratory frame, and the conventions we use (a) when the axis of symmetry of the forcing lay close to the x_3 axis of the laboratory frame, and (b) when the axis of symmetry lay close to x_1 axis of the laboratory frame. The coordinate system (x_1, x_2, x_3) is fixed in the laboratory frame, and the coordinate system (r_1, r_2, z) is fixed with respect to the symmetry of the forcing.

symmetry as axial quantities, and those with radial separations as radial quantities. For example, $f(x_1)$ is denoted as $f(z)$ when the axis of symmetry of the forcing lay along x_1 , and is called an axial quantity. In keeping with the geometry described above, our ‘axial’ measurements were in reality about 15° away from the axis of symmetry, and the ‘radial’ measurements were about 4° from its normal.

In the first part of this paper, we discuss measurements made at a single point of all three orthogonal components of velocity. For these measurements, both probes observed a fixed volume (aligned to within $10\ \mu\text{m}$) close to the centre of the soccer ball, which is the point $(0, 0, 0)$ in the coordinate system shown in figure 4. One probe measured a single component of the particle velocities, namely $\tilde{u}_{x_1}(0, 0, 0)$. The second probe measured two orthogonal components of the particle velocities, namely $\tilde{u}_{x_2}(0, 0, 0)$ and $\tilde{u}_{x_3}(0, 0, 0)$. For measurements described in the second part of this paper, we aligned the probes in a similar way, except that we positioned the second probe at different stations along the

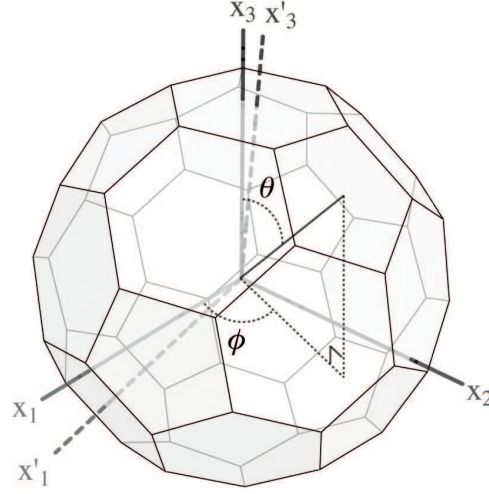


FIGURE 4. The schematic shows the coordinate system in the laboratory frame. \hat{x}_3 was aligned with the vertical. The axis of symmetry of the forcing lay along either x'_1 or x'_3 , depending on the experiment. Our measurements were made at points along x_1 .

x_1 axis, using a programmable linear traverse. This probe now measured $\tilde{u}_{x_2}(x_1, 0, 0)$ and $\tilde{u}_{x_3}(x_1, 0, 0)$. In addition, the single-velocity-component probe was rotated 90° to measure $\tilde{u}_{x_3}(0, 0, 0)$, which was coincident with one of the components measured by the two component probe when x_1 equaled zero.

For each of a series of forcing anisotropies, A , given by equation 2.1, we collected two data sets. For one data set, we aligned the axis of symmetry of the forcing close to x_3 , and for the other, we aligned the symmetry axis close to x_1 . For each value of the large-scale anisotropy, and each orientation of the symmetry axis, we collected data with the two-component LDV probe stationed at various positions along the x_1 -axis. We varied the anisotropy while fixing the quantity

$$K = \frac{1}{2} \left[\langle u_{x_1}^2(0, 0, 0) \rangle + \langle u_{x_2}^2(0, 0, 0) \rangle + \langle u_{x_3}^2(0, 0, 0) \rangle \right], \quad (2.2)$$

where the fluctuating parts of the velocities, \tilde{u}_i , are denoted by u_i , and $\langle \cdot \rangle$ denotes

Velocity Statistics (m s ⁻¹)	Axis Orientation	
	<i>z</i> '	<i>x</i> '
$U_{x_1}(0, 0, 0)$	0.099	0.14
$U_{x_2}(0, 0, 0)$	0.0055	-0.0044
$U_{x_3}(0, 0, 0)$	-0.038	0.027
$\sigma_{x_1}(0, 0, 0)$	0.99	0.99
$\sigma_{x_2}(0, 0, 0)$	0.98	0.98
$\sigma_{x_3}(0, 0, 0)$	0.96	0.98

TABLE 2. Three-component velocity statistics for symmetric forcing, measured at the centre of the soccer ball. The symbols U indicate the mean flow and the symbols σ indicate the RMS velocity fluctuations.

temporal averaging. In other words, we fixed the turbulence kinetic energy in the centre of the ball.

3. Anisotropy, axisymmetry and homogeneity

Three-dimensional velocity measurements made at single points in the centre region of the soccer ball show that the flow was approximately homogeneous and axisymmetric. Furthermore, the anisotropy of the turbulent velocity RMS fluctuations followed the anisotropy of the forcing signal. For the case of spherically symmetric forcing, with $A = 1$ (see equation 2.1), we expected and indeed found that the turbulence was isotropic. In this case, the components of the fluctuating velocity were each approximately 1 m s⁻¹, and the mean velocity was less than 0.15 m s⁻¹, or less than 15% of the fluctuations, as shown in Table 2.

Figure 5 shows the ratio of axial to radial velocity fluctuations as a function of the forcing anisotropy, A . Hereafter, we refer to $\langle u_i^2(z, r_1, r_2) \rangle^{1/2}$ as $\sigma_i(z, r_1, r_2)$, and σ_i as

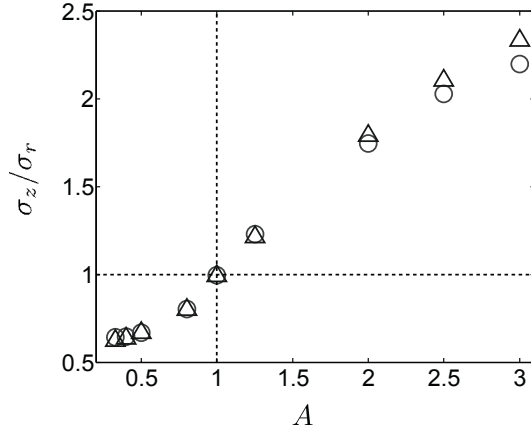


FIGURE 5. Velocity fluctuation ratios as a function of the forcing anisotropy, A . \circ is σ_z/σ_{r1} and \triangle is σ_z/σ_{r2} . Data were collected with the axis of symmetry lying along x'_3 . We obtained similar results (not shown) when the axis of symmetry lay along x'_1 .

$\sigma_i(0,0,0)$. Clearly the anisotropy of the turbulence followed the variation of A . In addition, the anisotropy was nearly the same whether measured in the r_1 or r_2 directions. Thus the turbulence was close to cylindrically symmetric, though this was less so at extreme values of A . The degradation in the cylindrical symmetry might be explained by the fact that the number of loudspeakers doing most of the work to drive the turbulence decreased as the value of A moved away from one. This is the nature of the forcing algorithm described before. As the number of loudspeakers effectively decreased, the turbulence probably became more sensitive to mechanical differences between the speakers, and to misalignments of the nozzles.

Next, we consider the degree to which the axisymmetry was spatially uniform. To test this, we evaluate how the velocity fluctuation ratios vary with distance from the centre of the soccer ball. Figure 6(a) shows the ratio of the two radial fluctuating velocities, $\sigma_{r2}(0,0,z)/\sigma_{r1}(0,0,z)$, at various distances from the centre of the ball along the axial direction. Within 50 mm, the values of this ratio deviated by less than 10% from 1, which indicates that the turbulence was close to cylindrically symmetric. Figure 6(b)

A	0.33	0.4	0.5	0.8	1.0	1.25	2.0	2.5
σ_z (m s ⁻¹)	0.74	0.75	0.79	0.91	1.08	1.21	1.42	1.47
σ_{r_2} (m s ⁻¹)	1.26	1.24	1.27	1.19	1.15	1.03	0.83	0.75
σ_z/σ_{r_2}	0.59	0.60	0.63	0.77	0.94	1.17	1.71	1.97
K (m ² s ⁻²)	1.87	1.83	1.92	1.82	1.91	1.79	1.69	1.65
$ U_z/U_{r_2} $	0.31	0.16	0.13	0.15	4.04	2.57	7.58	23.9
$ U $ (m s ⁻¹)	0.17	0.18	0.13	0.10	0.05	0.07	0.14	0.24
$\langle u_{r_1} u_{r_2} \rangle / (\sigma_{r_1} \sigma_{r_2})$	-0.07	-0.06	-0.06	-0.07	-0.07	-0.05	0.01	0.04
$\langle u_z u_{r_2} \rangle / (\sigma_z \sigma_{r_2})$	-0.06	-0.07	-0.06	-0.07	-0.07	-0.06	-0.01	0.02
ϵ (m ² s ⁻³)	5.4	4.9	5.4	6.0	6.7	7.0	6.5	6.4
η (μm)	163	167	163	159	155	153	156	156
τ_η (ms)	1.7	1.8	1.7	1.6	1.5	1.5	1.6	1.6

TABLE 3. The table shows the turbulence parameters, for various loudspeaker RMS amplitude ratios (A). The quantity K is the turbulent kinetic energy, $\frac{1}{2}(\sigma_z^2 + 2\sigma_{r_2}^2)$, and $|U|$ is $(U_z^2 + 2U_{r_2}^2)^{1/2}$. Data were collected at the centre of the soccer ball when the axis of symmetry was horizontal. We obtained similar results (not shown) when the axis of symmetry was vertical.

shows the ratio of the axial fluctuating velocity to one of the radial fluctuating velocities, $\sigma_z(r_1, 0, 0)/\sigma_{r_2}(r_1, 0, 0)$. The values at $r_1 = 0$ correspond to the values shown in figure 5. Again, the velocity fluctuation ratio is approximately constant within 50 mm of the centre of the ball. We infer that the anisotropy was approximately uniform within a central region with radius 50 mm.

To evaluate the homogeneity of the turbulent fluctuations, we show measurements of $\sigma_{r_2}(0, 0, z)/\sigma_{r_2}(0, 0, 0)$ and $\sigma_z(r_1, 0, 0)/\sigma_z(0, 0, 0)$ in figures 7(a) and (b). These quantities compare the amplitudes of the velocity fluctuations at locations away from the centre to those in the centre. Within a radius of 50 mm, the difference between

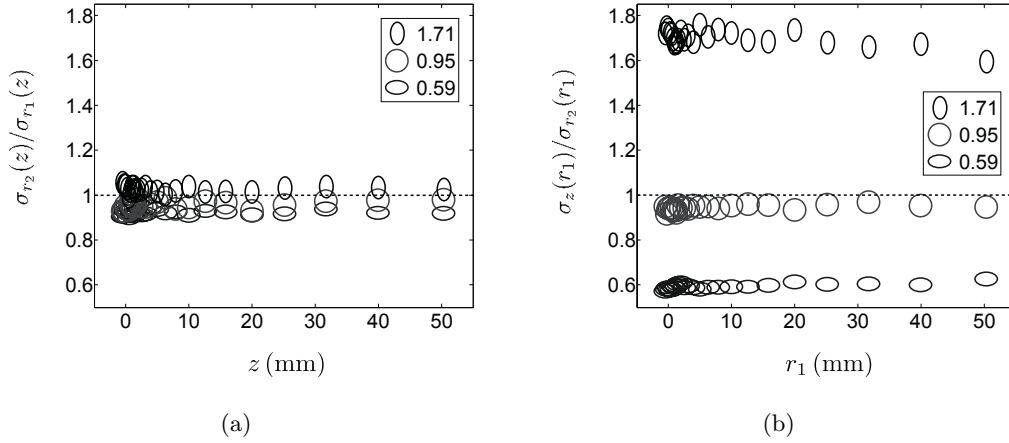


FIGURE 6. To demonstrate homogeneity of the turbulence axisymmetry, we show (a) the ratio of the two radial components of the velocity fluctuations, $\sigma_{r_2}(0, 0, z)/\sigma_{r_1}(0, 0, z)$, and (b) the ratio of the axial fluctuations to the radial fluctuations, $\sigma_z(r_1, 0, 0)/\sigma_{r_2}(r_1, 0, 0)$, at various stations moving away from the centre of the ball. The values in the legends, and in all other legends in this paper, are those of the data in (b) for $r_1 = 0$.

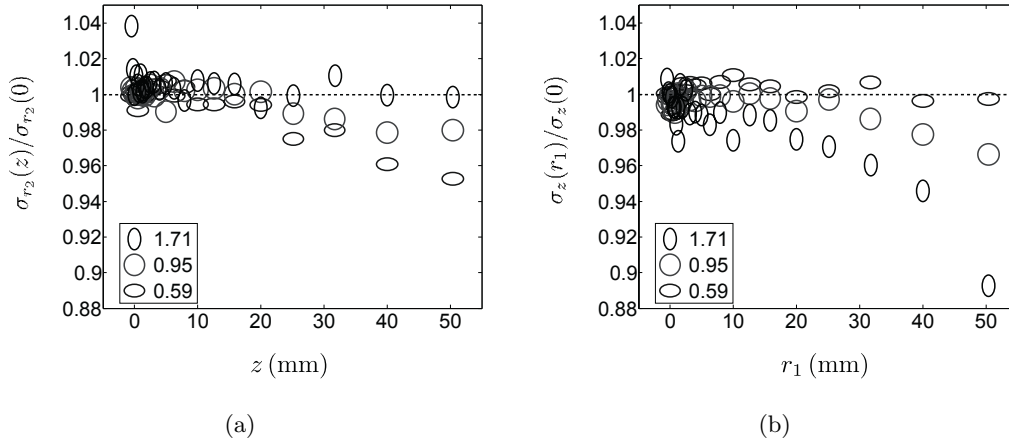


FIGURE 7. To demonstrate homogeneity of the turbulent fluctuations, we show (a) the radial fluctuations at positions along the axis, $\sigma_{r_2}(0, 0, z)/\sigma_{r_2}(0, 0, 0)$, and (b) the axial fluctuations at positions normal to the axis, $\sigma_z(r_1, 0, 0)/\sigma_z(0, 0, 0)$. As in figure 6, the values in the legend are the anisotropies measured at the centre of the soccer ball.

$\sigma_{r_2}(0, 0, z)/\sigma_{r_2}(0, 0, 0)$ and its value at the origin was within 5% of the value at the origin. The inequality also held for $\sigma_z(r_1, 0, 0)/\sigma_z(0, 0, 0)$.

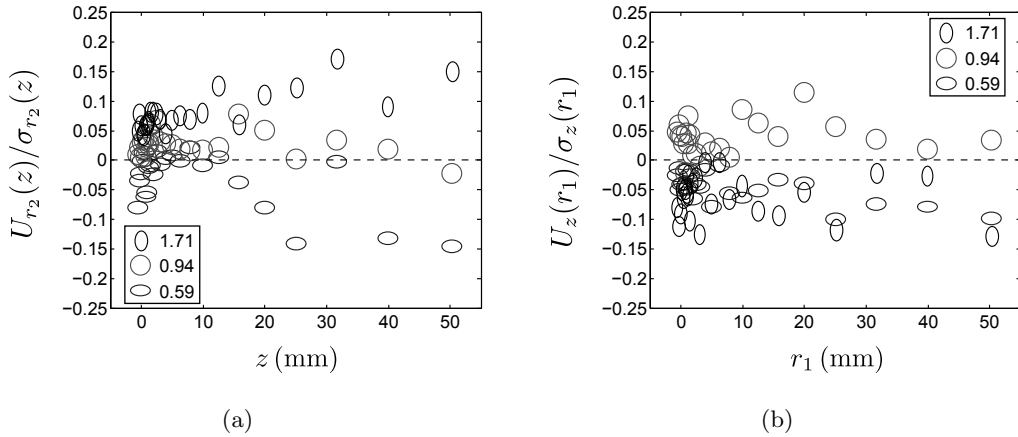


FIGURE 8. The mean flow in two directions as a fraction of the fluctuating velocities in those directions. The values in the legend are the anisotropies measured at the centre of the soccer ball.

Anisotropy can manifest itself not only in the fluctuations, but also through spatial variation of the mean velocity. In figures 8(a) and (b), we show the ratios of the mean flow velocities to the velocity fluctuations, $U_{r_2}(0, 0, z)/\sigma_{r_2}(0, 0, z)$ and $U_z(r_1, 0, 0)/\sigma_z(r_1, 0, 0)$. The shape of the curves are difficult to interpret, but may indicate that the natural centre of the turbulence was offset from the centre of our coordinate system. We concluded that variation in the mean velocity was negligible because it was typically more than ten times smaller in magnitude than the fluctuations, so that the energy in the mean flow was less than 1% of that in the fluctuations. Only at the extreme values of the anisotropy was the mean velocity as much as 15% of the fluctuations, which may have been due to the sensitivity of the turbulence to small differences between the speakers in this range of anisotropies, as discussed above.

Turbulence production by a mean shear is gauged by the Reynolds stresses, or the cross correlations between orthogonal velocity components. We measured two such stresses, $\langle u_{r_1}(0, 0, z) u_{r_2}(0, 0, z) \rangle$ and $\langle u_z(r_1, 0, 0) u_{r_2}(r_1, 0, 0) \rangle$, at various locations, z and r_1 , along

the two axes. The stresses were less than 7% of the corresponding kinetic energies, $\sigma_{r_1} \sigma_{r_2}$ and $\sigma_z \sigma_{r_2}$, respectively, and so had a only a small influence on the flow.

4. Universality in the second order velocity structure functions

We first use the transverse structure functions, defined by equations 1.2 and 1.3, to estimate the Reynolds number of the turbulence. In figure 9, the structure functions $D_{zz}(r_1)$ and $D_{r_2r_2}(z)$ are normalized by the Kolmogorov scaling. That is, we solve the equations for ϵ , the dissipation rate. Here, we assume that the Kolmogorov constant has the value given by Sreenivasan (1995), $C_2 = 2.1$, which is the mean of values taken from a collection of experimental studies. We assess the validity of this assumption later. We take the peak value of the function as our definition of the dissipation rate of the flow. The values estimated from $D_{r_2r_2}(z)$ are given in table 3. The corresponding values estimated from $D_{zz}(r_1)$ differ from those estimated from $D_{r_2r_2}(z)$ by no more than 13%. The dissipation rates depended slightly on the driving and reached a value of $6.7 \text{ m}^2\text{s}^{-3}$ for the case of isotropic turbulence. Under isotropic forcing, the Taylor scale was then $\lambda = \sqrt{15 \nu \sigma^2 / \epsilon} = 6.7 \text{ mm}$, where ν is the kinematic viscosity of air at room temperature ($1.57 \times 10^{-5} \text{ m}^2 \text{ s}^{-1}$), and the spherically averaged RMS velocity fluctuations was then $\sigma = \sqrt{(\sigma_z^2 + 2\sigma_r^2)/3}$, which gave a Taylor-microscale Reynolds number of $R_\lambda = \lambda \sigma / \nu = 481$. The Reynolds numbers for the anisotropic cases were similar.

We defined a scale-dependent measure of anisotropy, $D_{zz}(r_1)/D_{r_2r_2}(z)$ where $r_1 = z$. The data are shown in figure 10. Local isotropy requires that $D_{zz}/D_{r_2r_2}$ approaches one at small scales. In the limit of large separations, the ratio should approach σ_z^2/σ_r^2 , since the velocities $u_i(\mathbf{r})$ and $u_i(0)$ are uncorrelated when \mathbf{r} is large enough. Although we did not observe this regime, the values of the ratio in anisotropic cases did separate from the isotropic value as if to approach the values σ_z^2/σ_r^2 at larger, unobserved, scales.

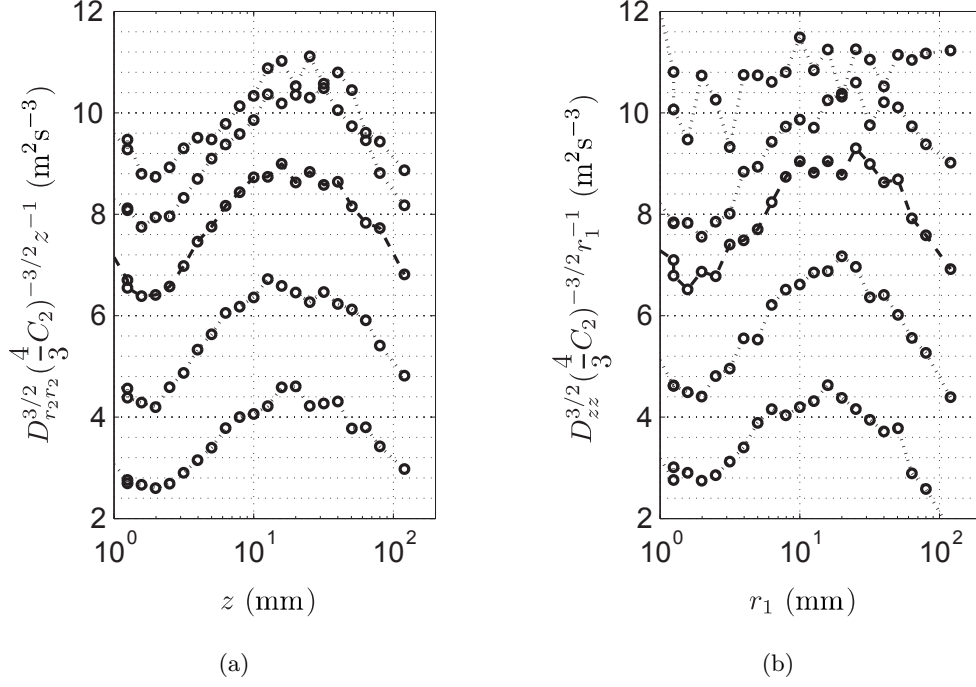


FIGURE 9. In (a) and (b), the axial structure functions, $D_{r_2 r_2}(z)$, and radial structure functions, $D_{zz}(r_1)$, are normalized by Kolmogorov's inertial range predictions given by equations 1.3 and 1.2. In order from bottom to top, the anisotropy, σ_z/σ_r , was 0.59, 0.77, 0.94, 1.16 and 1.98. Each curve was shifted by $1.5 \text{ m}^2 \text{ s}^{-3}$ with respect to the one below it (except the bottom one). The figure shows that we observed local isotropy, within the experimental error, for separations smaller than about 50 mm. This approach to isotropy, then, is a consequence of the velocity correlations inherent in the dynamics of turbulence. We extract further information from the structure function ratio through two interpretations, described below.

Because the structure functions do not exhibit clear scaling, as is evident in figure 9, we employ ESS to extract scaling exponents. We employed it in a new way, to compare the structure functions measured in different directions, rather than to compare structure

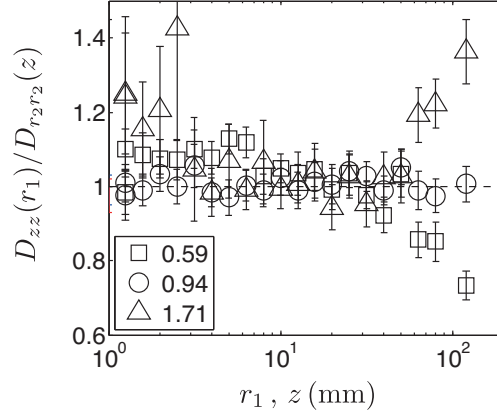


FIGURE 10. The ratios between structure functions in different directions but in the same flow, $D_{zz}(r_1)/D_{r_2r_2}(z)$, approach the isotropic value of one as the separation $r_1 = z$ decreases. Note that noise became important below separations of about 4 mm, as can also be seen in figure 9. Results for data taken at other values of the large-scale anisotropy are consistent with those shown here. The values in the legends are the anisotropy, σ_z/σ_r , measured at the centre of the soccer ball.

functions of different orders. According to Benzi *et al.* (1995), ESS implies that

$$D_{ii} = A^{(j)} \left(\frac{x_j}{L} f \left(\frac{x_j}{\eta} \right) \right)^{\zeta_2^{(j)}}, \quad (4.1)$$

where L is a large scale of the flow and $A^{(j)}$ are unknown constants. For standard ESS, one finds that the function $f(x_i/\eta)$ is independent of the order of the structure function.

We assumed that it is also independent of the direction in which the structure function is measured. In this way, we assumed isotropy of the function f , but not of the underlying scaling. It follows that

$$\frac{D_{zz}(r_1)}{D_{r_2r_2}(z)} = \frac{A^{(r)} \left((r_1/L) f(r_1/\eta) \right)^{\zeta_2^{(r)}}}{A^{(z)} \left((z/L) f(z/\eta) \right)^{\zeta_2^{(z)}}} = A' r_1^{\zeta_2^{(r)} - \zeta_2^{(z)}} = A' r_1^{\Delta \zeta_2}. \quad (4.2)$$

whenever r_1 equals z . The ratio is a form of ESS because it eliminates the influence of the function f in order to reveal the underlying scaling set by the exponents $\zeta_2^{(j)}$. To determine $\Delta \zeta_2$, we fit power laws to the data in figure 10 in the region between 4 and

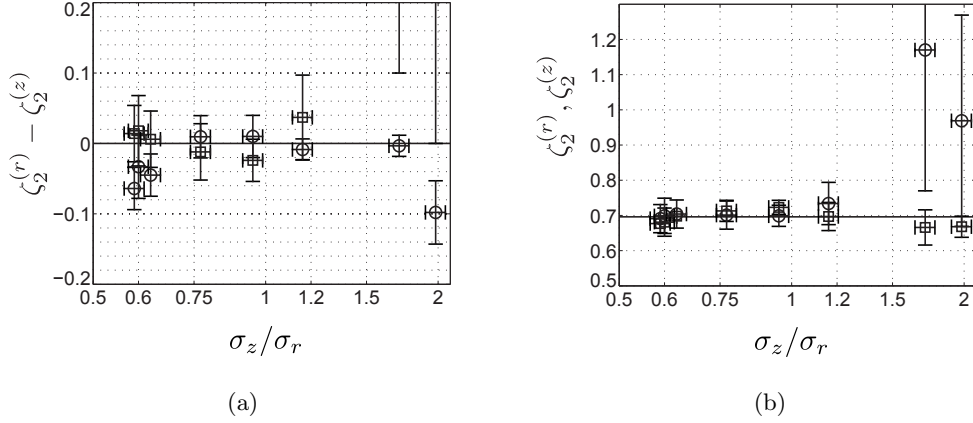


FIGURE 11. In (a), the \circ symbols are the scaling exponent differences measured through the use of equation 4.2. For the \square symbols, the differences were computed through the use of equation 4.3. Two data points above the top of the plot are out of view in order to make the deviations of the other points more visible. The values of these two points are 0.5 ± 0.4 and 0.3 ± 0.3 in order of increasing anisotropy. The exponents measured using equation 4.3 are shown in (b). Here, the \circ and \square symbols mark radial and axial scaling exponents, respectively.

40 mm, the lower bound being set by the appearance of noise in the data, and the upper bound by the emergence of the large-scale cutoff. It can be seen in figure 11(a) that the dependence of $\Delta\zeta_2$ on the anisotropy is non-monotonic.

Figure 11(a) also shows exponent differences derived from standard ESS. In the original expression of ESS,

$$D_{ii} \sim D_{iii}^{\zeta_2^{(j)}}, \quad (4.3)$$

where D_{iii} is the third moment of the absolute value of the velocity difference, $\langle |u_i(x_j) - u_i(0)|^3 \rangle$. For ESS to be present, $D_{iii} = B_i(r/L) f(r/\eta)$. In figure 12, we plot D_{zz} against D_{zzz} , and $D_{r_2r_2}$ against $D_{r_2r_2r_2}$, in order to uncover the scaling exponents $\zeta_2^{(r)}$ and $\zeta_2^{(z)}$, respectively. We fit power laws to the data in figure 12 for r and z between 4 and 40 mm, as before. The exponents of these power laws are shown in figure 11(b). Note that for two exponents measured in the radial direction of prolate spheroidal turbulence, the

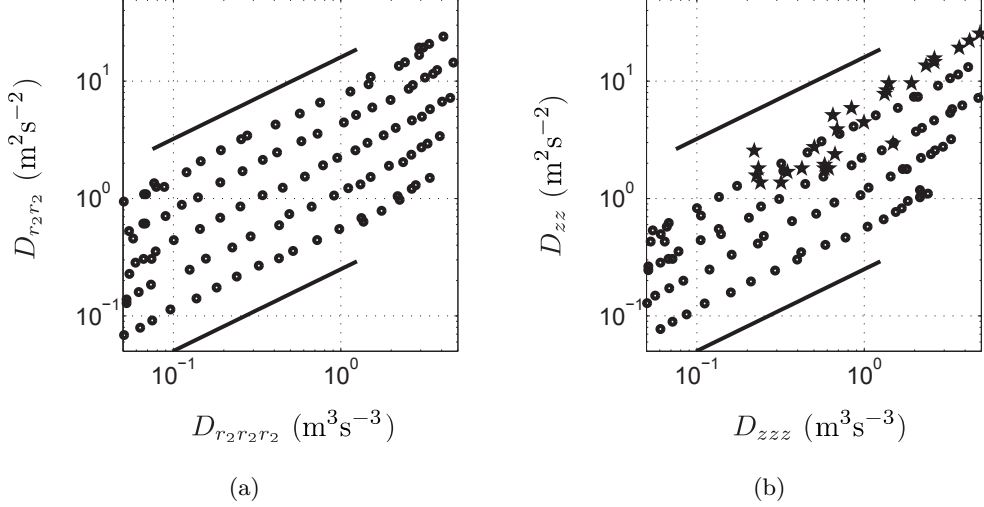


FIGURE 12. In (a) and (b), the axial structure functions, $D_{r_2 r_2}(z)$, and radial structure functions, $D_{zz}(r_1)$, are plotted against their third-order counterparts. For each curve in order from bottom to top, the anisotropy, σ_z/σ_r , was 0.59, 0.77, 0.94, 1.16 and 1.98. Each curve was shifted by a factor of 2 with respect to the one below it (except the bottom one). The solid lines are power laws with an exponent of 0.70. The uppermost curve in (b) is marked with stars in order to make the data distinguishable from the other data. For these data, the third order structure function did not converge.

data were insufficient to bring about convergence of the third order structure functions. This is evident in the scatter present in the corresponding data in figure 12. We note speculatively that for these two conditions, the Reynolds stresses were about 0.08 higher than for all of the other cases, as seen in table 3, and that this may point to a role for shear in altering the scaling.

As seen in figure 11(b), the dependence of the scaling exponents, $\zeta_2^{(r)}$ and $\zeta_2^{(z)}$, on anisotropy was non-monotonic. Furthermore, deviations of $\Delta\zeta_2$ from zero measured using standard ESS do not follow the same trend as the those measured through equation 4.2. This discrepancy suggests that anisotropy is by itself not responsible for the deviations, but that they have their origin in measurement noise and error. The mean value of the

scaling exponents, excluding the two outliers, was 0.70 ± 0.03 . This value is the same as the one found by Benzi *et al.* (1995) in a wind tunnel at comparable Reynolds number, and the value is indicated with a horizontal line in the figure.

Shen & Warhaft (2002) found that the exponent of the second order transverse structure function was 0.1 smaller in the direction normal to the mean flow in a wind tunnel, both with and without shear. Wind tunnel turbulence is approximately axisymmetric in the absence of shear, with the axis of the tunnel corresponding to our z . Although one of our data points, namely the one for $\sigma_z/\sigma_r = 1.98$, does fall at -0.1 , in agreement with Shen & Warhaft (2002), their result cannot be reconciled with the body of our data.

Let us consider the Kolmogorov constant. We calculated the ratio $C_2^{(r)}/C_2^{(z)}$ in two ways. First, we computed an average of the structure function ratio, $\langle D_{zz}(r)/D_{r_2r_2}(z) \rangle$, shown in figure 10. The average was taken over a range of separations that bracketed the peak in the compensated structure functions, or $4\text{mm} < r_1, z < 40\text{mm}$. In the inertial range, according to equations 1.2 and 1.3,

$$\frac{D_{zz}(r_1)}{D_{r_2r_2}(z)} = \frac{\frac{4}{3}C_2^{(r)}(\epsilon r_1)\zeta_2^{(r)}}{\frac{4}{3}C_2^{(z)}(\epsilon z)\zeta_2^{(z)}} = \frac{C_2^{(r)}}{C_2^{(z)}} \quad (4.4)$$

when $r_1 = z$, $\zeta_2^{(r)} = \zeta_2^{(z)}$, and because the dissipation, ϵ , is a scalar quantity. We used the standard deviation in the value of the ratio as a measure of the error of the measurement. The second method was designed to mimic the one usually employed to measure C_2 (or ϵ) when data are collected in only one direction. That is, we estimated each C_2 from the maximum of the compensated structure functions. In order to reduce the influence of noise, we found the maximum of a polynomial function, second-order in $\log(r)$, fit to the data between 4 and 40 mm. The ratio between the maxima, $\max(D_{zz}(r)/r^{2/3})/\max(D_{r_2r_2}(z)/z^{2/3})$, was then calculated. As before, the quantity is an estimate for the ratio of Kolmogorov constants because the dissipation rate cancels. We used the deviation of the data from the fitted parabolas to estimate the error. Al-

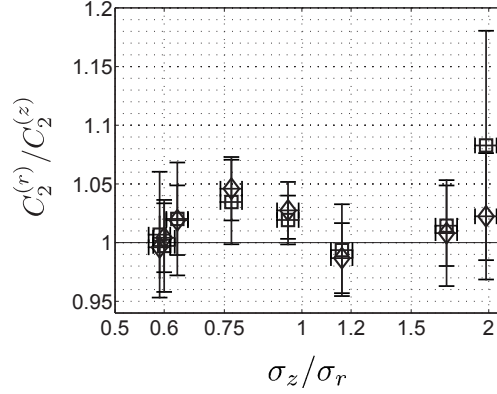


FIGURE 13. The ratio between Kolmogorov constants measured in different directions, $C_2^{(r)}/C_2^{(z)}$. The \diamond symbols are the ratio between the maximum values of the compensated radial and axial structure functions. The \square symbols are $\langle D_{zz}(r_1)/D_{r_2r_2}(z) \rangle$, the ratio of radial to axial structure functions averaged over a range of scales $4 < r_1, z < 40$ mm.

though each method described here suffers from limitations, they both serve as practical definitions of $C_2^{(r)}/C_2^{(z)}$.

The two measures of $C_2^{(r)}/C_2^{(z)}$ are plotted in figure 13. The ratios deviated from the isotropic value by up to 4%, except for one outlier whose value was about 8% higher than 1.0. The observed dependence on the anisotropy, if there was one, was non-monotonic. However, Buša *et al.* (1997) found in a shell model of turbulence that the Kolmogorov constant varied monotonically with anisotropy. Although they predicted a dependence too weak to detect in our data, it is reasonable to expect one that is qualitatively similar. Since we did not see such a monotonic dependence, we concluded that the deviations of the Kolmogorov constants from isotropy were probably not due to the anisotropy in the fluctuations, but were rather the result of measurement noise and error. Though large, the uncertainty in our data is smaller than the scatter seen in the data collected by Sreenivasan (1995), whose amplitude is about 10%. It follows that anisotropy in the

velocity fluctuations alone does not account for the variation in previously measured values of the Kolmogorov constant.

5. Conclusions

We investigated systematically the influence of anisotropic agitation on the inertial scales of turbulence in an experiment with Taylor-based Reynolds number $R_\lambda = 481$. Thirty two loudspeaker-driven jets pointed toward the centre of a spherical chamber and were driven to produce axisymmetric turbulence, which in a central volume had no shear, no mean flow, and was homogeneous. We observed flows for which the ratio of axial to radial RMS velocity fluctuations was between 0.6 and 2.3. We found that the anisotropy of the velocity fluctuations at the largest scales had the same anisotropy as the agitation. According to two inertial range measures, the second order velocity structure functions were independent of anisotropy. There was extended self-similarity, and the structure functions had the same scaling exponent in different directions and for different anisotropies, 0.70 ± 0.03 . The Kolmogorov constant, C_2 , also showed no dependence on the anisotropy. Because of this, we expect anisotropic corrections, such as those uncovered by the $SO(3)$ decomposition (e.g. Kurien & Sreenivasan 2001; Biferale & Procaccia 2005), to be smaller than the error in our measurements (about 4%). This holds unless the anisotropic corrections cancelled in the two directions we measured, an outcome we consider unlikely. Further experiments are necessary to determine whether deviations from isotropy present within the uncertainty of our measurement are significant.

This research was supported by the Max Planck Society and was carried out in cooperation with the International Collaboration for Turbulence Research. We thank Lance Collins, Zellman Warhaft, K.R. Sreenivasan and Reginald Hill for valuable suggestions. We thank Mathieu Gibert for drawing our attention to the work of Fox *et al.* (1988).

Kelken Chang acknowledges financial support from the Deutsche Forschungsgemeinschaft (German Science Foundation) through the grant XU91/3-1.

REFERENCES

- ALBRECHT, H.-E., BORYS, M., DAMASCHKE, N. & TROPEA, C. 2003 *Laser Doppler and phase Doppler measurement techniques*. Berlin Heidelberg: Springer.
- ANDERECK, C. D., LIU, S. S. & SWINNEY, H. L. 1986 Flow regimes in a circular couette system with independently rotating cylinders. *J. Fluid Mech.* **164**, 155–183.
- BENZI, R., CILIBERTO, S., BAUDET, C. & CHAVARRIA, G. R. 1995 On the scaling of three-dimensional homogeneous and isotropic turbulence. *Physica D* **80**, 385–398.
- BENZI, R., CILIBERTO, S., TRIPICCIONE, R., BAUDET, C., MASSAIOLI, F. & SUCCI, S. 1993 Extended self-similarity in turbulent flows. *Phys. Rev. E* **48**, R29–R32.
- BEWLEY, G. P., SREENIVASAN, K. R. & LATHROP, D. P. 2008 Particles for tracing turbulent liquid helium. *Exp. Fluids* **44**, 887–896.
- BIFERALE, L. & PROCACCIA, I. 2005 Anisotropy in turbulent flows and in turbulent transport. *Phys. Rep.* **414**, 43–164.
- BUCHHAVE, P. 1975 Biasing errors in individual particle measurements. In *Proc. LDA Symp. Copenhagen, Tonsbakken 16-18, 2740 Skovlunde, Denmark*, pp. 258–278.
- BUCHHAVE, P., GEORGE JR., W. K. & LUMLEY, J. L. 1979 The measurement of turbulence with the laser-Doppler anemometer. *Ann. Rev. Fluid Mech.* **11**, 443–504.
- BUŠA, J., HNATICH, M., HONKONEN, J. & HORVATH, D. 1997 Stability of kolmogorov scaling in anisotropically forced turbulence. *Phys. Rev. E* **55**, 381–394.
- COMTE-BELLOT, G. & CORRSIN, S. 1966 The use of a contraction to improve the isotropy of grid-generated turbulence. *J. Fluid Mech.* **25**, 657–682.
- FOX, R. F., GATLAND, I. R., ROY, R. & VEMURI, G. 1988 Fast, accurate algorithm for numerical simulation of exponentially correlated colored noise. *Phys. Rev. A* **38**, 5938–5940.
- GLEZER, A. & AMITAY, M. 2002 Synthetic jets. *Annu. Rev. Fluid Mech.* **34**, 503–529.
- GOEPFERT, C., MARIÉ, J.-L., CHAREYRON, D. & LANCE, M. 2010 Characterization of a system

- generating a homogeneous isotropic turbulence field by free synthetic jets. *Exp. Fluids* **48**, 809–822.
- HUSSEIN, H. J., CAPP, S. P. & GEORGE, W. K. 1994 Velocity measurements in a high-reynolds-number, momentum-conserving, axisymmetric, turbulent jet. *J. Fluid Mech.* **258**, 31–75.
- HWANG, W. & EATON, J. K. 2004 Creating homogeneous and isotropic turbulence without a mean flow. *Exp. Fluids* **36**, 444–454.
- KOLMOGOROV, A. N. 1941 Local structure of turbulence in an incompressible fluid at very high Reynolds numbers. *Dokl. Akad. Nauk SSSR* **30**, 299–303.
- KURIEN, S. & SREENIVASAN, K. R. 2001 Measures of anisotropy and the universal properties of turbulence. In *NATO Advanced Study Institute. Les Houches Session LXXIV. New Trends in Turbulence. Turbulence: Nouveaux Aspects*, pp. 53–111.
- LU, J., FUGAL, J. P., NORDSIEK, H., SAW, E. W., SHAW, R. A. & YANG, W. 2008 Lagrangian particle tracking in three dimensions via single-camera in-line digital holography. *New J. Phys.* **10**, 125013.
- OUELLETTE, N. T., XU, H., BOURGOIN, M. & BODENSCHATZ, E. 2006 Small-scale anisotropy in Lagrangian turbulence. *New J. Phys.* **8**, 102.
- SADDOUGHI, S. G. & VEERAVALLI, S. V. 1994 Local isotropy in turbulent boundary layers at high Reynolds number. *J. Fluid Mech.* **268**, 333–372.
- SHEN, X. & WARHAFT, Z. 2002 Longitudinal and transverse structure functions in sheared and unsheared wind-tunnel turbulence. *Phys. Fluids* **14**, 370–381.
- SREENIVASAN, K. R. 1995 On the universality of the Kolmogorov constant. *Phys. Fluids* **7**, 2778–2784.
- STAIKU, A., VORSELAARS, B. & VAN DE WATER, W. 2003 Turbulence anisotropy and the so(3) description. *Phys. Rev. E* **68**, 046303–1 – 046303–12.
- TAVOULARIS, S. & CORRISIN, S. 1981 Experiments in nearly homogeneous turbulent shear flow with uniform mean temperature gradient. part 1. *J. Fluid Mech.* **104**, 311–347.
- VOTH, G. A., LA PORTA, A., CRAWFORD, A. M., ALEXANDER, J. & BODENSCHATZ, E. 2002 Measurement of particle accelerations in fully developed turbulence. *J. Fluid Mech.* **469**, 121–160.

- WARNAARS, T. A., HONDZO, M. & CARPER, M. A. 2006 A desktop apparatus for studying interactions between microorganisms and small-scale fluid motion. *Hydrobiologia* **563**, 431–443.
- WEBSTER, D. R., BRATHWAITE, A. & YEN, J. 2004 A novel laboratory apparatus for simulating isotropic oceanic turbulence at low Reynolds number. *Limnology and Oceanography: Methods* **2**, 1–12.
- YEUNG, P. K. & BRASSEUR, J. G. 1991 The response of isotropic turbulence to isotropic and anisotropic forcing at the large scales. *Phys. Fluids A* **3**, 884–897.
- ZIMMERMANN, R., XU, H., GASTEUIL, Y., BOURGOIN, M., VOLK, R., PINTON, J.-F. & BODENSCHATZ, E. 2010 The lagrangian exploration module: An apparatus for the study of statistically homogeneous and isotropic turbulence. *Rev. Sci. Instrum.* **81**, 055112.